Polyethylene/Graphene-Nanoplatelets Nanocomposites with Improved Thermo-Chemical Stability: The Role of Surface Polarity of Graphene-Nanoplatelets

Hamidreza Ghadami Karder[a], Gholamreza Pircheraghi[a*]

a Polymeric Materials Research Group (PMRG), Department of Materials Science and Engineering, Sharif University of Technology, Tehran, Iran.

* Corresponding author E-mail address: pircheraghi@sharif.ir

Preprint not peer reviewed

This preprint research paper has not been peer reviewed. Electronic copy available at: https://ssrn.com/abstract=4698229

Abstract

Throughout the world, polyethylene (PE) pipes are widely used for the distribution of drinking water. As a result of exposure to drinking water containing ClO_2, practical experience has demonstrated that the lifetime of PE pipes can be significantly reduced, and PE pipes in water distribution systems may prematurely fail. In recent years, graphene nanoplatelets (GNP) have been proven to be capable of absorbing free radicals and slowing down the degradation of polymers. In this research, the effect of GNP polarity and concentration upon PE100 polyethylene stability against chemical degradation in chlorinated water has been explored. A high-polarity—synthesized using electrochemical exfoliation—and a low-polarity GNP—commercially available—were used. According to the results, low-polar GNP contributes to the stabilization of polyethylene against thermo-chemical degradation without damaging its short-term properties. Low-polar GNP is an ideal additive for improving the short-term and long-term properties of polyethylene resins as well as extending the service life of PE pipes in water distribution systems.

Keywords: Polyethylene, Nanocomposite, Graphene nanoplatelet (GNP), Thermo-chemical degradation, Chlorine dioxide.

Preprint not peer reviewed

This preprint research paper has not been peer reviewed. Electronic copy available at: https://ssrn.com/abstract=4698229

1. Introduction

Polyethylene (PE) products has long been used in many aspects of modern society, such as buildings, transportation, and the drinking water distribution network [1]. This is due to their acceptable mechanical properties, excellent corrosion resistance, ease of production, low manufacturing costs, high flexibility, and etc. [2]. Due to the widespread use of PE, high density polyethylene (PE100) pipes have been utilized in place of metal pipes as a pipe material for a large number of water distribution networks operating at pressures up to 16 bar [3, 4].

Chlorine-containing disinfectants are commonly used within municipal water distribution systems in order to eliminate the possibility of microorganisms contaminating potable water [5, 6]. Due to the growing interest in chlorine dioxide (ClO_2) as an effective drinking water disinfectant in recent years, its influence on the long-term mechanical properties and durability of the piping system is important. In comparison to chlorine-free disinfectants and monochloramine, chlorine dioxide is more powerful than any other disinfectant due to its oxidizing power, which eliminates viruses and chlorine-resistant pathogens as well as preventing biofilm formation [5]. It is therefore possible to attribute the significant antioxidant degrading capability of ClO_2 to its one-electron oxidant nature. When a phenol is oxidized by one electron, it produces a radical cation and a phenoxyl radical as a result [7-9]. Because of the hindered nature of the phenolic ring in Irganox 1010 (tert-butyl groups), the corresponding phenoxyl radical is more inclined to undergo a B-cleavage at the side chain [7, 9]. Consequently, quinoid structures are formed as a result of this process [9]. Following the oxidation of the antioxidative compounds (hindered phenols) to the quinoid structure and chloride quinoid structure, ClO_2 migrates to the hydrocarbon polymers and causes deterioration of the material. The diffusion of ClO_2 was found to be responsible for controlling the aging process

Preprint not peer reviewed

This preprint research paper has not been peer reviewed. Electronic copy available at: https://ssrn.com/abstract=4698229

of PE in Colin et al.'s extensive research [10, 11]. In addition to having a strong reactivity toward organic materials, ClO_2 also has a weak reactivity toward hydrocarbons, which makes it unable to remove hydrogen from hydrocarbons [9, 12, 13]. The oxidation reactions that occur directly between chlorine dioxide and polyethylene are controversial [9]. In accordance with the work of Myhstrad et al. [14], a mechanism of reaction between organic compounds and ClO_2 has been proposed. One electron gain result in the formation of chlorite ions (ClO_2^-) as the main reaction product [15]. As a result of this reaction, chlorate (ClO_3^-) and chloride (Cl^-) ions are formed in under 30 percent, depending on the pH of the solution [16]. Because of the steric hinderance imposed by the hydrate shell, it is likely that ions generated by the various reactions of ClO_2 in water will diffuse very slowly into the polymer. In addition, ions have a negligible effect on the PE degradation process, especially in deeper material layers [15]. Under typical water conditions, saturated aliphatic hydrocarbons and aliphatic olefins are not reactive with chlorine dioxide [9, 12, 17]. Lindgren et al. [18, 19] stated that allylic hydrogen can be captured by chlorine dioxide, resulting in intermediates of free radicals in the reaction between chlorine dioxide and some olefins. Furthermore, Yu et al. [20] presented data on pipes made of polyethylene that were exposed to chlorine dioxide-containing water (4 ppm) under 90 ^oC and pH 6.8 that demonstrated the high resistance of saturated hydrocarbons to ClO_2. No detectable IR absorption was recorded beneath the degradation layer as a result of carbonyl, hydroxyl, or chlorine groups [20]. Polyethylene is subjected to degradation on its surface when the antioxidant system is completely depleted. Hydrogen abstraction occurs when radicals with high reactivity (e.g., hydroxyl, $ClO2^-$, $ClO3^-$, and Cl^- radicals) react with the polymer on its immediate surface [7, 9]. Following hydrocarbon radical formation, peroxyl radicals are generated by oxygen, which subsequently oxidizes polymer molecules, according to Bollande-Gee [21, 22]. During oxidation, polyethylene's

Preprint not peer reviewed

This preprint research paper has not been peer reviewed. Electronic copy available at: https://ssrn.com/abstract=4698229

molecule-to-molecule continuity gradually disappears [7]. As a result, cracks appear in the new material when stress is applied to the structure [7]. According to colin et al. [11], testing under tensile conditions revealed that brittleness occurs as the weighted average molar mass (M_W) gets close to a threshold of 70 $kgmol^{-1}$.

It has been widely reported that nanosheets of graphene and graphene oxide (GO) have recently been employed in the polymer industry as reinforcement to enhance the functionality of polymers because of their incredible properties in terms of thermal, mechanical properties, and electrical characteristics [23, 24]. Further, graphene is an exceptional material because it exhibits a powerful intrinsic antioxidant effect, which shows significant potential for enhancing the stability of polymers against thermal and oxidative deterioration [25]. Studies that have been conducted by Liu et al. [26] have also demonstrated that TRGO's scavenging ability for free radicals does not exclusively depend on the concentration of sp^2 structure. Instead, it depends on the dimensions of the sp^2 hybrid regions that are continuously connected. Several factors have contributed to the improvement of thermo-oxidative durability in nanocomposites. These factors include the tortuous path effect against oxygen molecules, free radical scavenging ability, physical barrier effect on degradation product emission, and improvements in thermal conductivity [27, 28]. A number of graphene-based polyethylene terephthalate [29], polymethyl methacrylate [30], and polyamide 6 [28] have demonstrated notable improvements in thermo-oxidative durability. As observed by Liu et al. [26], By removing oxygen containing groups (OCGs) from TRGO, the sp^2 hybrid regions gradually get more complete and increasingly larger, resulting in a declining fluorescence effect and enhanced radical scavenging capabilities. As a result of too high reduction temperature (T_r), such as 1000 °C, the sp^2 hybrid domains will become damaged and will develop holes on a macro level. This will result in a loss of structural regularity and radical scavenging activity. Using high

Preprint not peer reviewed

This preprint research paper has not been peer reviewed. Electronic copy available at: https://ssrn.com/abstract=4698229

temperature annealing, Yuan et al. [24] investigated the effects of heteroatoms doped with nitrogen, phosphorus, and boron on the crystalline structure of a reduced graphene oxide (RGO). According to the study, doped RGO can significantly increase PP thermal resistance. Heteroatom doping affected the electronic structure of RGO, which had a significant impact on the thermal and oxidative stability of PP nanocomposites.

This study demonstrates graphene's efficacy in enhancing thermo-oxidative stability performance on un-stabilized PE100 and illustrates the cooperative stabilization mechanism between antioxidants and graphene nanoplatelets (GNP). To minimize the impact of inherent additives, un-stabilized PE100 powder was used as the matrix. However, to the extent of our knowledge, no research has been conducted on the influence of GNP (the amount of oxygen-containing groups), as well as the dispersion state of nanofillers on the mechanical and thermal properties of high-density polyethylene (PE100). In this work, we present and compare the mechanical and thermal characteristics of two nanocomposite materials made by melt blending PE100 with two nanofillers: synthesized graphene nanoplatelets (SG) and commercial graphene nanoplatelets (CG). To understand the concept of synergistic stabilization, we investigated the dispersion of SG/CG in PE100 matrix. As a further experiment, 1-1-diphenyl-2-picrylhydrazyl radicals (DPPH) were used to examine the radical scavenging capabilities of SG, CG, and AO.

1. Experimental

1.1. Materials

The bimodal PE100 powder (HMCRP100N), Irganox1010 antioxidant (AO1010), and Irgafos168 antioxidant (AO168) were provided by Jam Petrochemical Co., Iran. A flexible graphite sheet with a thickness of 320 microns was supplied by Jiangxi DASEN Technology Co. This graphite sheet

Preprint not peer reviewed

This preprint research paper has not been peer reviewed. Electronic copy available at: https://ssrn.com/abstract=4698229

served as an anode for the electrochemical synthesis of graphene nanoplatelets (SG sample code). Sodium sulfate, DMF (99.5 %wt.), and nitric acid (70%wt.), sodium chlorite, and sodium bisulfate monohydrate were purchased from Merck. A platinum plate (10 x 10 x 0.23 mm) was used as a cathode in electrochemical synthesis. The filter paper with Model No. 42 was supplied by Whatman. The graphene nanoplatelets (CG) were purchased from Kara Pajuhesh Amirkabir Co. A stock solution of chlorine dioxide (ClO_2) was prepared by mixing 5 grams of powdered sodium chlorite and sodium bisulfate monohydrate each in screw-capped transparent glass jars, then 250 mL of distilled water into the solution. It took 2 hrs to complete the reaction and stock solutions were maintained at 4 ^oC in the dark.

1.2. Synthesis of SG sample

The synthesized graphene nanoplatelets (SG) was prepared based on electrochemical exfoliation method [31, 32]. The flexible graphite sheet was carefully cut into 1 x 5.2 cm pieces with a pair of scissors. The platinum plate was immersed in a diluted aquatic solution of HNO_3 (15% wt.) to remove contamination and surface oxides, followed by washing and drying in an oven at 50°C. 0.2 M electrolyte was synthesized by adding 2.48 g of Na_2SO_4 to 87.5 ml of deionized water. During electrochemical synthesis, the graphite electrode was positioned next to the platinum (Pt) electrode at a fixed spacing of 3 cm. During the first stage of electrochemical synthesis, a constant bias voltage of 5 V was applied for 4 minutes in order to facilitate the intercalation of SO_4^{2-} ions. As the bias voltage was increased to 10V, the graphite exfoliated and electrochemical synthesis was completed after approximately 60 minutes. In the following step, after the exfoliation process has been completed, the powders were collected and washed using a vacuum filtration system [32]. The powders were subsequently dispersed in deionized water, followed by freeze-drying.

Preprint not peer reviewed

This preprint research paper has not been peer reviewed. Electronic copy available at: https://ssrn.com/abstract=4698229

1.3. Nanocomposite Sample Preparation

Table 1. Sample code names and formulations

Batch name	AO1010 (ppm)	AO168 (ppm)	SG (ppm)	CG (ppm)
HDPE	2000	1000	-	-
HD1SG	2000	1000	1000	-
HD3SG	2000	1000	3000	-
HD6SG	2000	1000	6000	-
HD1CG	2000	1000	-	1000
HD3CG	2000	1000	-	3000
HD6CG	2000	1000	-	6000

HDPE/GNP nanocomposites and HDPE sample (reference sample) were prepared using a laboratory internal mixer (Brabender Intelli-Torque Plasti-Corder). Prior to melt compounding, HDPE powder and GNP were dried at 70 ^{o}C for an hour. For each batch, predetermined amounts of HDPE powder, GNP, AO1010, and AO168 were thoroughly stirred together in a beaker according to Table 1, using a spatula to achieve homogeneity. Afterward, the homogeneous mixture was added to the melt compounder and allowed to mix for five minutes directly. The mixing temperature and rotation speed were adjusted to 190°C and 60 rpm, respectively. The melt compounds were compression molded into 100 x 100 x 1 mm^3 sheets at 180 ^{o}C for 5 min at pressure of 300 bar by using a 30-tonnage manual hot press (SPH-300, Santam Co., Iran), followed by air cooling to room temperature. In order to investigate the effect of GNP on the oxidative induction time (OIT) and the synergistic stabilization of antioxidants, the concentrations of

Preprint not peer reviewed

This preprint research paper has not been peer reviewed. Electronic copy available at: https://ssrn.com/abstract=4698229

primary (AO10010) and secondary (AO168) have been selected based on the research of Dordinejad et al [33].

2. Accelerated Ageing procedure

Twelve dumbbell-shaped samples were cut from HDPE and HDCG samples and placed in aging solutions of DI water containing 5 ppm of ClO_2 disinfectant. The jars were cap-sealed and positioned in a temperature-controlled oven at 50 ^oC. The samples were collected periodically for laboratory testing to examine the deterioration of samples under a variety of exposure conditions. The aging parameters were held constant for 1200 h and the solutions were refreshed periodically for 48 h at a constant ClO_2 concentration. Through the use of a spectrophotometer (Jenway 6705 UV/Visible Scanning Spectrophotometer), the concentrations of the solutions and free chlorine were monitored in accordance with Method 10069.

4. Characterization

The powder X-ray diffractograms of the GNP samples were obtained using PANalytical (XPert Pro MPD) with CuKa radiation (k = 1.5406A°). The background was corrected by OriginPro to obtain higher-quality output. The distance between layers (d) was calculated via Bragg's law, and the mean size of crystals (t) was determined by the Debye-Scherrer equation for each sample. The number of layers in each sample was determined using the equation (n=t/d). Thermo-gravimetric analyses (TGA) were carried out on SG and CG samples by TGA TA Q600 under Ar atmosphere from ambient temperature to 600 ^oC at a temperature increment of 10 ^oC /min. XPS spectra were obtained using BESTEC (EA 10) spectrometer and the survey spectra were recorded by step of 1.45 eV. Mg Ka X-ray radiation with 200W energy was used as the excitation source. An analysis of the morphology of the dried powders was carried out using field emission scanning electron

Preprint not peer reviewed

This preprint research paper has not been peer reviewed. Electronic copy available at: https://ssrn.com/abstract=4698229

microscopy (FESEM, TeScan - Mira III machine). The morphology of GNP was analyzed by Transmission Electron Microscopy (Zeiss EM900). For TEM images, GNP were dispersed in ethanol and sonicated for 5 minutes. Few drops of these suspensions were dried on holey carbon grids. According to [34], the DPPH assay was employed to assess CG and SG's free radical scavenging capabilities. Small modifications to the method were made. At first, 1900 µl of 0.1 mM DPPH solution in ethanol were injected into 100 µl of samples at various concentrations (i.e., 32.5, 62.5, 125, 250, and 500 mg/ml for CG, SG, and AO1010) in DMF at 25°C. The solution was left to stand in darkness for 30 minutes after mixing. After 30 minutes of incubation, the absorbance was determined at 517 nm using a UNICO2000 spectrophotometer and named abs(sample). 1900 µl of DPPH solution plus 100 µl DMF was used as a control sample and the absorbance was named abs(control). The inhibition rate of radical scavenging capacity (RSC) can be written as Equation 1:

$$\%RSC=\frac{abs(control)-abs(sample)}{abs(control)} \times 100 \qquad \text{Equation 1}$$

Through linear regression of plots in which the horizontal axis showed sample concentrations and the vertical axis represented the arithmetic mean antioxidant activity percent from five independently conducted tests, the EC50 values (expressed as the amount of antioxidant needed to reduce the initial DPPH concentration by 50%) of AO1010, SG, and CG were determined. Regression analysis revealed high determination coefficients ($R>0.95$). The mechanical properties of the dumbbell-shaped specimens were tested through tensile testing with a Hounsfield machine (H10KS). Dog bone specimens were die-cut from molded sheets in accordance with ASTM D638, sample type V. The uniaxial tensile tests were done at 50 mm/min displacement until failure or rupture took place. Three samples were analyzed for each composition and for each duration of

Preprint not peer reviewed

This preprint research paper has not been peer reviewed. Electronic copy available at: https://ssrn.com/abstract=4698229

ClO_2-exposure. Stress-strain curves were calculated and allowed the determination of tensile properties such as tensile strength, yield strength, break strength, and elongation. The rheological properties of nanocomposites were assessed with a stress-controlled rheometer MCR 501 Anton Paar in response to angular frequency and nano-filler loading. Experimental measurements were made at an isothermal temperature of 190 ^oC under small-amplitude oscillation shear mode using parallel plate geometry (25 mm diameter). The 1 mm thick sample disks were manufactured under the same conditions as those used for 100 x 100 x 1 mm^3 sheets. Storage modulus (G′), loss modulus (G″), and complex viscosity of the nanocomposites were monitored at 1 % strain (linear viscoelastic region) from 0.1 to 100 Hz frequency. The polydispersity index (PDI) was measured according to the Equation 2 [35-37]:

$$PDI=\frac{100000}{G^{'}(\omega_{COP})}\ ,\ \omega_{COP}=\omega\ (G^{'}=G^{''}) \qquad \text{Equation 2}$$

A frequency sweep test determines the crossover frequency by crossing the storage modulus and loss modulus on a log-log scale, where G′ is the storage modulus and G″ is the loss modulus. The oxidation induction time (OIT) measurements were performed using a Differential Scanning Calorimeter (TA Q20) according to the standard method (ISO 11357-6, 2002). The specimen was kept in an aluminum pan. The temperature was then raised to 210°C and held for 5 minutes under nitrogen atmosphere. Then the gas stream was switched to an oxygen atmosphere at a flow rate of 50 mL/min. Each sample's OIT value was derived from its time interval between oxygen charging and the oxidation reaction. In order to examine the level of dispersion of GNPs in nanocomposite films, optical microscopy was performed using an Olympus BX51. The images were analyzed with ImageJ software for determining the size of the agglomerates. For this regard, approximately 1 mg of nanocomposite film was loaded between two glass slides and compressed at 200 °C on a

Preprint not peer reviewed

This preprint research paper has not been peer reviewed. Electronic copy available at: https://ssrn.com/abstract=4698229

hot plate for 5 minutes, and then air-cooled to room temperature. Field-emission scanning electron microscope (FE-SEM) was used to examine the dispersion of the fillers in the PE matrix at the cryo-fractured surface and the surface after exposing to water containing ClO_2 through a TeScan - Mira III field emission microscope. To avoid charge buildup, sample surfaces were sputter-coated with gold.

3. Results and discussions

3.1. Characterization of GNPs

XRD method was employed to determine the structural characteristics of SG and CG samples. Fig. Fig. 1 illustrates the XRD patterns of SG and CG. In order to determine the distance between layers (d), the mean crystallite size (t), and the quantity of stacked layers (n), Bragg and Scherrer's equations were applied. The proportion of each phase, interlayer d-spacing, crystallite thickness, and number of layers was calculated and the attained results are shown in Table 2. As shown in Fig. 1-a, asymmetric and wide peaks around 25° can be deconstructed into two peaks by using Gaussian peaks fitted to the curve using background-subtracted XRD data from SG. Consequently, the intense peak at 26.7° belongs to multilayer graphene (MLG) and the one at a lower angle belongs to few-layer graphene (FLG). The peak at 11° is attributed to GO. Table 2 and Fig. 1. indicate that the product of Na_2SO_4 electrolyte (SG sample) contains 52% FLG (6 layers), 22% MLG (23 layers), and 26% GO (2 layers). However, there are no peaks of FLG or MLG in CG and the sample is predominantly made up of MLG (120 layers).

To determine the magnitude of functional groups on the GNP surface, thermal gravimetric analysis (TGA) of SG and CG was conducted in an argon atmosphere. Fig. 1-c illustrates the results. It is believed that the weight loss associated with SG under 150 °C is due to the desorption of water

Preprint not peer reviewed

This preprint research paper has not been peer reviewed. Electronic copy available at: https://ssrn.com/abstract=4698229

stored in "stacked" structures [32]. A comparison of the CG sample with the SG sample shows almost no water molecules trapped between the layers of CG; this may be because CG is composed of fewer oxygen-containing groups (OCG) than SG. SG's curve indicates weight loss at 150 °C should be related to loss of unstable oxygen-containing groups. Another at 350 °C, as previously reported, suggests additional degradation of OCGs, some of which can withstand temperatures up to 600 °C [32, 38]. There is a lower weight loss in the CG sample in the total weight loss area than the SG sample. This is due to the lower content of OCGs on the surface of the CG's layers. The following order can be proposed for the OCG content of the studied samples, after considering the loss of weight due to the decomposition of all OCGs up to 600°C: SG > CG.

Table 2. The distance between layers (d), crystallite size (t), quantity of layers (n) and the proportion of each phase of SG and CG samples

sample	d (Å)			t (Å)			n			Fraction of phase (%)		
	GO	FLG	MLG	GO	FLG	MLG	GO	FLG	MLG	GO	FLG	MLG
SG	9.12	3.43	3.35	13.9	22	76.1	2	6	23	26	52	22
CG	-	-	3.35	-	-	403.5	-	-	120	-	-	100

The XPS method is the most commonly used analytical method for analyzing the chemical composition of graphene-based materials. After subtracting the baseline from the results, the C/O atomic ratio can be determined. As a result, the C/O ratio of the CG sample is 25.3, which is significantly higher than the C/O ratio of the SG sample prepared through the electrochemical

Preprint not peer reviewed

This preprint research paper has not been peer reviewed. Electronic copy available at: https://ssrn.com/abstract=4698229

exfoliation protocol (Fig. 1-d). It can be seen from the XPS results that the CG sample has the lowest polarity, while the SG sample has the highest OCGs, thus having the highest polarity.

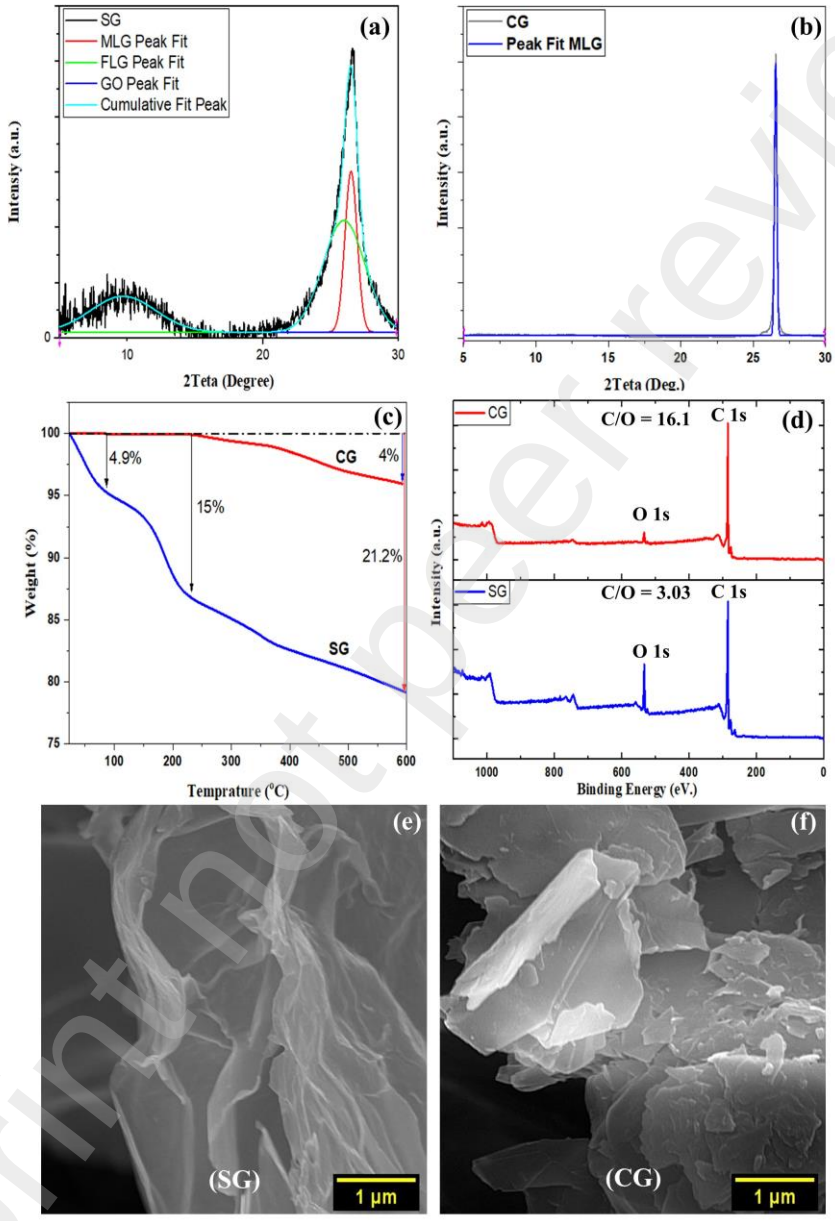

Fig. 1 XRD spectrum of (a) SG and Gaussian fitted curves, (b) CG samples and Gaussian fitted curves. (c) TGA graph of SG and CG samples. (d) XPS survey spectra of SG and CG samples. (e) and (f) FESEM images SG and CG samples.

Preprint not peer reviewed

This preprint research paper has not been peer reviewed. Electronic copy available at: https://ssrn.com/abstract=4698229

Images obtained by TEM can provide valuable insight into exfoliation and graphene sheet morphology. A mixture of multilayer graphene (black areas) and few-layer graphene (dotted zones) can be observed in Fig. S1-(a). As shown in Fig. S1-(a), the as-produced SG nanosheets are entangled with each other, forming a structure that resembles wrinkled paper. The oxidation reaction leads to a wide variety of imperfections and functional groups composed of sp3 hybridized carbon atoms. It appears that the semitransparent or transparent-looking SG flakes were synthesized in a similar manner to those synthesized by other researchers through the use of electrochemical techniques. A multilayer graphene structure can be seen in Fig.S1-(b), which is represented by black areas on the graphene flakes.

A comparison of the morphological properties of the SG and CG powder samples was performed by scanning electron microscopy. Representative images are shown in Figs. 1 (e) and (f), respectively. The SEM image of SG shows a transparent sheet-like morphology, while the CG sample has an agglomerated structure of wrinkled platelets.

According to recent studies, multiple varieties of nanoparticles are efficient antioxidants and free radical scavengers [24-27]. Studies focused on fullerenes [39] and carbon nanotubes [40] have also demonstrated that they are effective at scavenging reactive oxygen species (ROS). AO1010, SG, and CG have all been evaluated for their radical scavenging abilities using the DPPH assay. This assay is commonly used to quantify antioxidant activity against hydroxyl, alkyl, and peroxyl radicals. In Fig. 2, all of the samples display a continuous increase in scavenging activity as the sample concentration rises monotonously. The determined EC50 values for AO1010, SG, and CG are 352.5, 920.3, and 1213.3 mg/mL, respectively. This indicates that AO1010's radical scavenging activity is more effective even at lower concentrations than SG and CG, as expected.

Preprint not peer reviewed

This preprint research paper has not been peer reviewed. Electronic copy available at: https://ssrn.com/abstract=4698229

Antioxidant activity patterns vary depending on the graphene oxide structure or a few-layer graphene structure. According to some researchers, the antioxidant properties of carbon materials may be influenced by the formation of radical adducts at sp^2 sites, which delocalize spin within the conjugated graphene network and eliminate the radical upon forming the second adduct, via electron exchange, hydrogen transfer from functional groups, or by chelating transition metallic ions and inhibiting Fenton-based radical generation [41]. According to Qiu et al. [41], graphene with few layers has numerous scavenging sites than monolayer graphene oxide in spite of having a lower surface area. This suggests the main scavenging regions are the sp^2-carbon structure rather than oxygen-containing functional groups. According to researchers, GO is a weak hydrogen donor due to the nonphenolic nature of most hydrogen-containing OH groups. It is believed that these groups are located in basal sp^3-carbon regions that do not allow radical resonance stabilization following hydrogen donation [41]. According to Yang et al. [27], instead of reacting with the TrGO sheets during the assay, the DPPH probes may be physically attached to the surface. Therefore, Yang et al. [27] proposed that the DPPH value derived should be indicative of both the free radical adsorption by chemical and physical means on TrGO surfaces.

In accordance with XRD results, a large proportion of the SG sample is comprised of FLG, and the sp^2-carbon sites of FLG and MLG participate in neutralizing DPPH radicals. Additionally, DPPH radicals can also be absorbed onto the surfaces of GO sheets, which is another beneficial process to the value of radical scavenging capacity (RSC). Therefore, the DPPH value obtained in SG should represent the combined chemical contribution of FLG and physical adsorption of free radicals onto GO surface. The stacking of graphene layers in the CG sample results in a lower amount of sp^2 structure and a smaller number of continuous sp^2 hybrid domains involved in radical

Preprint not peer reviewed

This preprint research paper has not been peer reviewed. Electronic copy available at: https://ssrn.com/abstract=4698229

scavenging. The scavenging activity of samples can be written in the following order: AO1010 (EC50=352.5 µg/mL) > SG (EC50 = 920.3 µg/mL) > SG (EC50 = 1213.3 µg/mL).

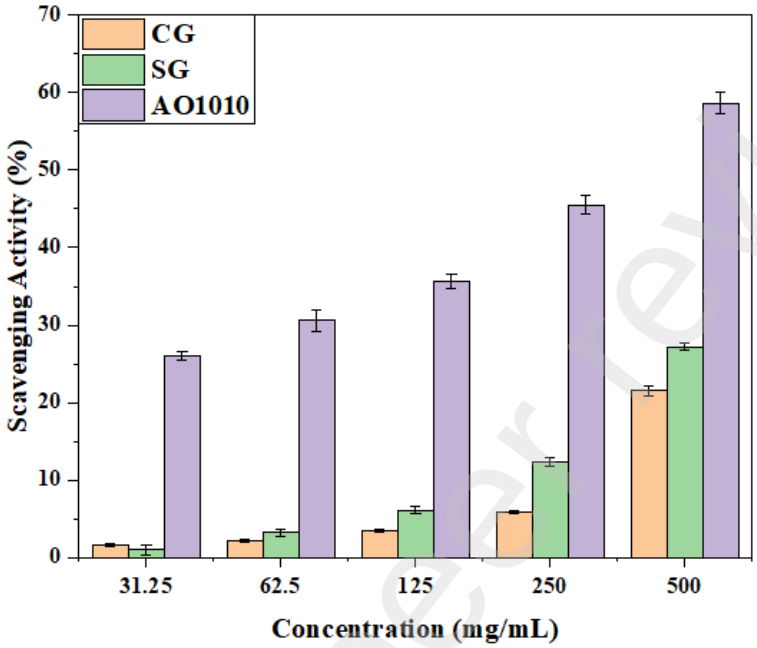

Fig. 2 The radical scavenging ability of AO1010, SG and CG toward DPPH free radical.

2.2. Characterization of Nanocomposites

2.2.1. Microscopy analysis

Nanoparticle dispersion and strong interacting with nanofillers and polymers are well known contributors to enhancing the physicochemical properties of polymer nanocomposites [27, 42]. Field-emission electron scanning microscopy (FESEM) was used to study SG and CG dispersion in HDPE as well as interfacial interactions. Fig. 3 illustrates the cryogenically fractured surfaces of HD/SG and HD/CG nanocomposites.

Based on the FESEM micrographs of HD1CG, HD3CG, and HD6CG shown in Figs. 3-a, c, and e, it is evident that GNP is distributed more uniformly throughout the polymer matrix. There were

Preprint not peer reviewed

This preprint research paper has not been peer reviewed. Electronic copy available at: https://ssrn.com/abstract=4698229

no observed voids between the HDPE matrix and the GNP sheets as a result of the attachment of the polymeric fibril to the GNP sheets. This indicates that nanoparticles have been widely dispersed within the PE matrix at the micron-scale and the polymer matrix has completely surrounded the reinforcement sheets, resulting in a successful interaction between the polymer matrix and the GNPs. It is believed that strong interfacial adhesion improves stress transfer between the CG and polymer matrix, which in turn enhances mechanical performance. It should be noted that effective dispersion was achieved without the use of any compatibilizers. The shear forces generated in the internal mixer were sufficient to disperse the CG sheets within the PE matrix.

Figs 3-b, d, and f illustrate SEM micrographs of HD1SG, HD3SG, and HD6SG nanocomposites, respectively. As observed in Fig. 3-b, at low loadings of 0.1 %wt., there was better dispersion of GNP, and micro-sized stacks could be observed throughout the matrix. The addition of GNP, however, resulted in larger stacks and uneven particle dispersion in the matrix large stacks, particularly when loaded at high levels, may be the result of insufficient affinity between PE matrix and SG nanoplatelets. This has a significant role in GNP delamination. Based on the TGA and XRD results, due to the mismatch of surface polarity of SG and non-polar characteristic of PE's molecules, it can be considered that the affinity between high polar SG nanoplatelets is significantly higher than that SG and polymer matrix, resulting that SG are likely to aggregate under melt processing conditions.

Preprint not peer reviewed

This preprint research paper has not been peer reviewed. Electronic copy available at: https://ssrn.com/abstract=4698229

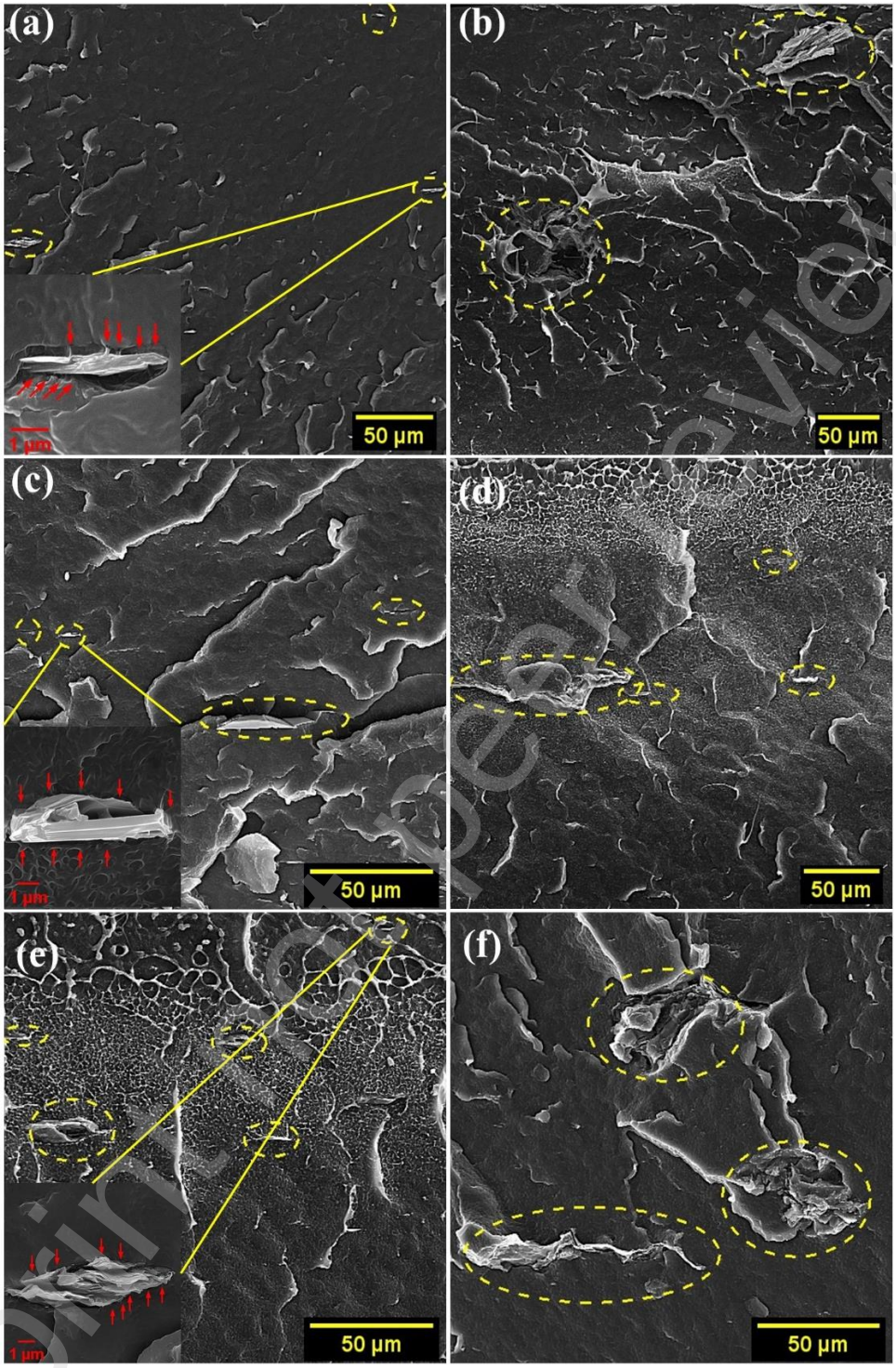

Fig. 3 The FE-SEM images of SG's dispersion in HD1SG, HD3SG, and HD6SG (a, b, c) (respectively) and CG's dispersion in (b, e, f) HD1CG, HD3CG, and HD6CG.

Preprint not peer reviewed

This preprint research paper has not been peer reviewed. Electronic copy available at: https://ssrn.com/abstract=4698229

Optical microscopy photomicrographs presented in Fig. 4 provide an evaluation of graphene nano platelets dispersion and distribution in the thin films on a micrometer scale in the continuous matrix of the PE100. The photomicrographs illustrate high contrast structures relating to GNP and very pale features relating to PE100 spherulite structure. As can be seen in Fig. 4, The CG have been dispersed more homogeneously throughout the PE100 matrix. However, some agglomerates of layers appear to be present at higher loading of CG sample, as shown in Fig. 4. With increasing the content of the SG to higher concentration (Up to 0.6%wt), the particles aggregate and get greater in size and a more ununiformed dispersion is observed. Aggregates are caused by Van der Waals interactions between GNPs in combination with the incompatible polarity between matrix and GNP. In order to achieve a suitable dispersion in the PE100 matrix, it is necessary to disperse the filler with strong shearing forces. In the case of HD3SG and HD6SG nanocomposites, melt-mixing shear forces are not sufficient to inhibit the aggregation of GNPs. According to park et al. [43], The relative dispersion index (RDI) can be defined as the area occupied with the GNP divided by whole area. A high relative dispersion index shows a more homogeneous dispersion throughout the matrix, because the fillers uniformly cover the total area of the photomicrographs. As shown in Fig. 4, The state of dispersion of these thin films demonstrates low polar CG powder show better dispersion than the high polar SG powder, which is inclined to reaggregate in the PE100 matrix.

Preprint not peer reviewed

This preprint research paper has not been peer reviewed. Electronic copy available at: https://ssrn.com/abstract=4698229

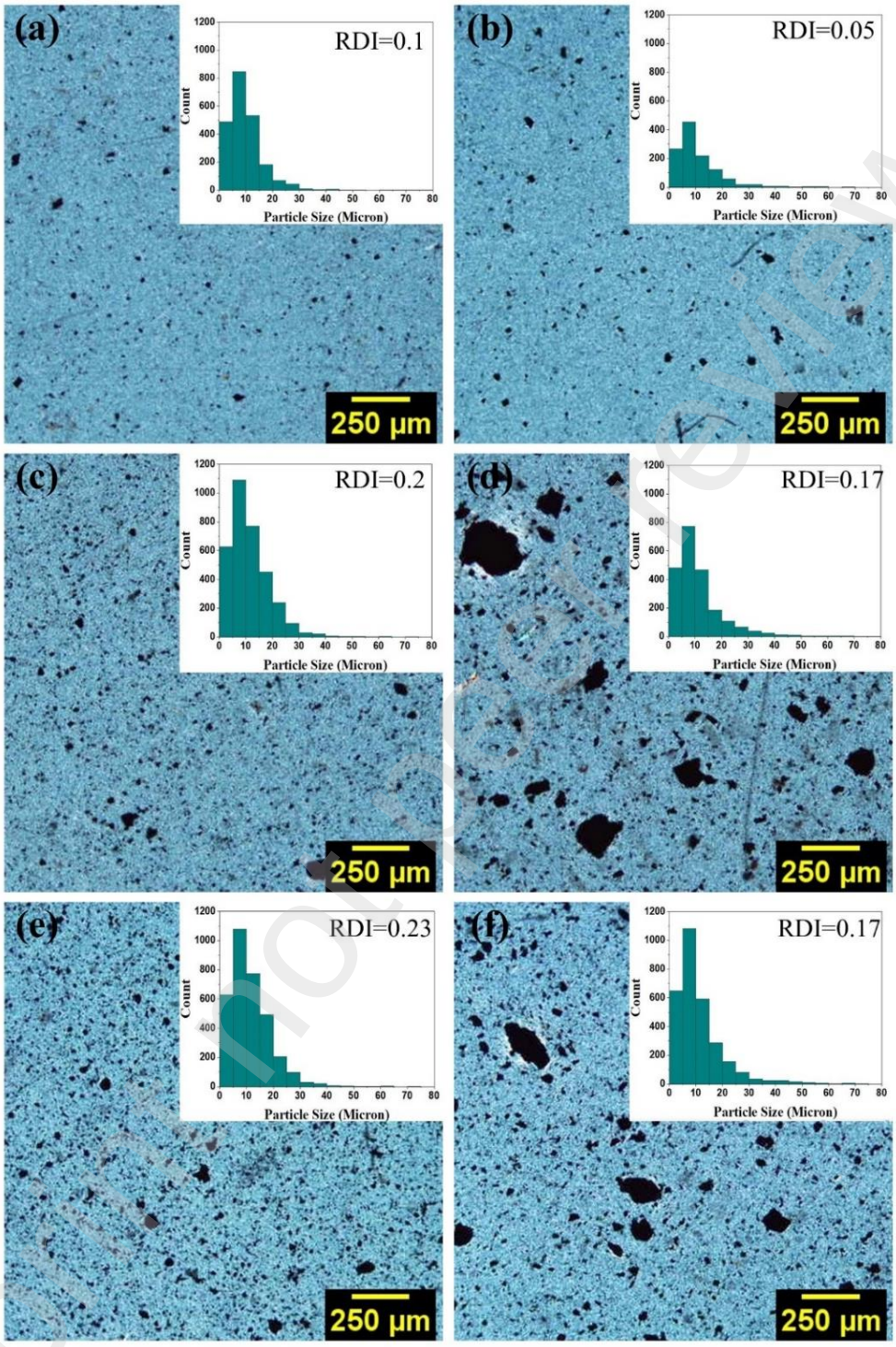

Fig. 4 Optical microscopy photomicrographs of CG's Dispersion in (a, c, e) HD1CG, HD3CG, and HD6CG and SG's dispersion in HD1SG, HD3SG, and HD6SG (b, d, f) (respectively).

Preprint not peer reviewed

This preprint research paper has not been peer reviewed. Electronic copy available at: https://ssrn.com/abstract=4698229

2.2.2. Thermal Measurements

OIT is used to evaluate the antioxidative efficiencies of GNP and antioxidants from DSC measurements, as presented in Fig. 5. As depicted in Fig.5, the OIT value of neat HDPE was 94.8 min. This means that AO can inhibit HDPE degradation due to its superior antioxidant activity. The OIT value was considerably raised to 111 min with 0.1 wt.% loading of CG. This indicates that PE100's thermo-oxidative stability has been noticeably enhanced with the 0.1 wt.% GNP loading. Additionally, the OIT value exhibited a descending trend with higher CG levels. When CG content was increased to 0.6 wt. %, an OIT value of 100.6 min was recorded, which was higher than that of HDPE matrix. Yang et al. [27] have concluded that nanocomposites' thermo-oxidative stability is dependent upon both radical scavenging capacity and GNP dispersion state. The decreasing of OIT can be attributed to the worsened dispersion of CG nanoplatelets at higher loadings.

The OIT value was markedly elevated to 106.5 min with the incorporation of a low amount (0.1 wt. %) of SG. However, the OIT of HD3SG and HD6SG did not increase even more by incorporating higher amounts of SG. As a result of the addition of 0.6 wt.% SG to the PE medium, the OIT value declined significantly to 87.4 min. This indicates that a high SG loading has a significant negative effect on PE thermo-oxidative stability. The intricate effects of SG addition on PE oxidative degradation arise from antioxidants in the PE matrix. Many researchers have recommended that antioxidants can be adsorbed on surface of nanoparticles such as RGO [44], Aluminum oxide [45], silica [46], montmorillonite [47], and carbon black [48], which decreases the antioxidant efficiency. Here, at low SG loading, antioxidant adsorption by SG may be barely noticeable. There is a synergistic effect between SG and antioxidants which inhibits PE oxidative

Preprint not peer reviewed

This preprint research paper has not been peer reviewed. Electronic copy available at: https://ssrn.com/abstract=4698229

degradation. However, there is a considerable potential for higher SG content to form large size and multilayer agglomerates. These agglomerates trap antioxidants efficiently to decrease antioxidative efficiency.

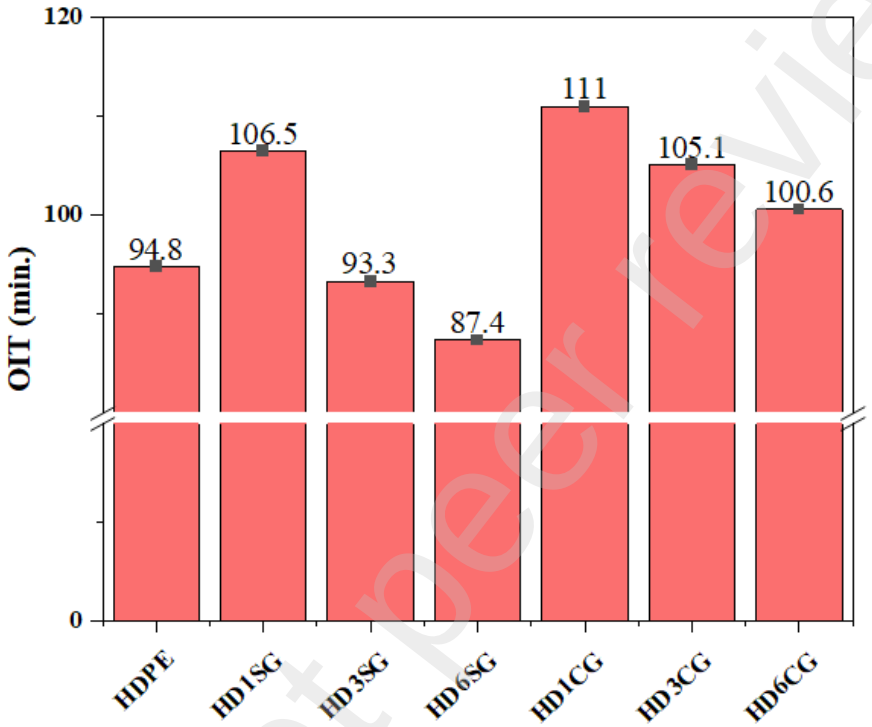

Fig. 5 determination of oxidation induction time (OIT) of neat HDPE, HD/SG, and HD/CG.

2.2.3. Mechanical and Rheological Measurements

The common stress–strain curves obtained from uniaxial tensile tests on pure HDPE, HDPE/SG, and HDPE/CG nanocomposites are illustrated in Fig. 6. In Fig.6, it is clearly visible that the average yield strength value for each SGs/CGs content is within the standard error limit. As reported, good CG dispersion and strong interfacial bonding are achieved in HD/CG nanocomposites. It is hypothesized that the enhancement of tensile strength without decreasing elongation is largely due to the exceptional mechanical performance of graphene, its efficient

Preprint not peer reviewed

This preprint research paper has not been peer reviewed. Electronic copy available at: https://ssrn.com/abstract=4698229

dispersion in the matrix, and robust interfacial interactions between the two components [49, 50]. The more effectively the nanofiller interacts with the matrix, the higher break elongation will be achieved. Elongation at break increases as a result of the mechanical interaction between graphene. The elongation of HDPE/CG nano composites was similar/higher than HDPE indicating that the filler dispersion was uniform. CG, however, has a negligible effect on tensile strength and nanocomposites is almost comparable to neat HDPE. Interestingly, the CG increased the elongation at break HD6CG by 66%. Since CG is more well-dispersed in the matrix polymer than SG. This elevation in tensile strain was potentially caused by exposure of pure polymer to high temperatures in the extruder. This occurred under a combination of shear and elongation forces. As a result, graphene nano platelets served the role of an antioxidant and prevented accelerated thermo-oxidative degradation of the polymer [35].

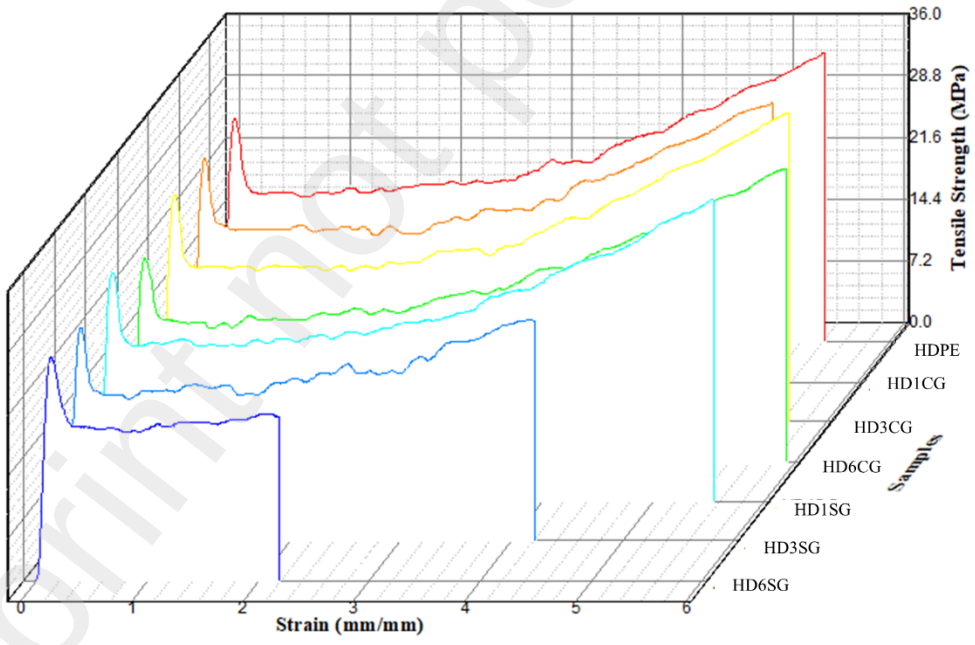

Fig.6. stress–strain curves of pure HDPE, HD/SG, and HD/CG nanocomposites.

Preprint not peer reviewed

This preprint research paper has not been peer reviewed. Electronic copy available at: https://ssrn.com/abstract=4698229

The elongation at break of HD/SG nanocomposites reduced in comparison with neat HDPE. For example, HD6SG drastically decreases elongation from 522% to 237%. The agglomerates can act as a source of stress concentration and crack propagation initiation points, thereby decreasing SG reinforcing efficiency [51]. Namely, in HD1SG, the SG sheets can be dispersed in the polymer matrix, while further loading will cause the SG sheets to stack together again due to the existence of the high interaction forces between high polar nanoplatelets. Therefore, the CG reinforcement efficiency is clearly superior to the SG. There are multiple potential explanations for this, including: According to SEM and TOM, the CGs are uniformly distributed throughout the matrix, but some large aggregates were observed in HDPE/SG. Tensile property values of pure HDPE, HD/SG, and HD/CG are depicted in Table S1 (Supporting Information).

Rheology under linear oscillatory shear is a widely used approach in polymer-based nanocomposites. A clear expression of storage (G') and loss (G") moduli of the polymer, as well as their frequency sensitivity, illustrates its viscoelastic properties as well as the effects of fillers on the polymer matrix. In order to determine the network-like structure, the dispersion state of the SG and CG fillers embedded in the polymer matrix, the ability of the SG and the CG fillers to limit the movement of the polymer chains, and the degree of interaction between the fillers and the polymer matrix, the rheological characteristics of HD/SG and HD/CG nanocomposites were examined. Rheological properties can also be used to determine the processing characteristics of polymer composites. As shown in Fig. 7, it is clear that with increasing SG/CG content at all frequency ranges (0.01-100 Hz), negligible changes can be seen in the storage modulus of HDPE-nanocomposites. Nonterminal characteristics at low frequencies can be related to the emergence of 3D networks of GNP, which leads to the restriction of polymer chains [52].

Preprint not peer reviewed

This preprint research paper has not been peer reviewed. Electronic copy available at: https://ssrn.com/abstract=4698229

From Fig. 7, it was found that the G' of SG/CG nanocomposite is almost the same as the neat HDPE, which means there is no occurrence of percolation threshold with increasing CG/SG content. The increased elasticity can affect the melt processing of the HDPE nanocomposite. For example, in pipe extrusion the high elasticity of the polymer melt can induce the surface instabilities including sharkskin and melt fracture [53]. Therefore, as shown in Fig. 7, both of GNPs do not have negative effect on melt processing of used PE100 for pipe extrusion.

However, the exact observation of the results may help to understand the interaction between polymer/filler and structure of the produced nanocomposites. The crossing modulus point (G_c) and crossing angular frequency point (ω_C) of nanocomposite samples have decreased as shown in Table 3. In other words, the mean relaxation time of the nanocomposite is sample increased due to hindrance of the chain movements because of GNP incorporation. Thus, with increase of the CG concentration from 0.1 wt.% to 0.3wt.%, the mean relaxation time is increased, while at higher concentration, 0.6 wt.%, it is decreased due to GNP aggregation and hence better chain movement.

It is accepted that the value off the cross over (G_c) point is related to molecular weight distribution and PDI based on equation 2 [35-37, 54]. The decrease of the G_c means the broadening of the MWD and vice versa as shown in table 3. Incorporating 0.1 wt.% of CG and SG significantly reduced G_c compared to other samples, while these samples show high OIT 111 and 106 min, respectively. This shifting to lower values after reinforcement implies that the polymer displayed a broader molecular weight distribution, which can be clearly observed from the increase in PDI [35-37, 54]. There is also a possibility that the shift in PDI upon the incorporation of reinforcement was caused by exposing the neat polymer to elevated temperatures, under the combined effects of shear and elongation forces, for an extended period of time. It is reported that during early stage of the thermo-oxidation degradation the MWD is narrowed, because of breakage of long chains to

Preprint not peer reviewed

This preprint research paper has not been peer reviewed. Electronic copy available at: https://ssrn.com/abstract=4698229

medium length chains [36]. Therefore, it can be expected that if sample is properly protected during melt processing its MWD is unchanged. In other words, the lower G_c means the wider MWD, which is expected for bimodal PE100, and the more effective antioxidant efficiency. As a result, the nanofiller in the polymer may induce a synergistic antioxidant action, which protected the polymer against thermo-oxidation degradation during melt processing. In contrast to neat bimodal HDPE, reinforced polymers have a higher polydispersity index (PDI). As a result of OIT analysis, the samples with higher OIT show the lower G_c or wider.

As shown in Figure 7-b and c, by increasing the amount of CG to values of 0.3 and 0.6, the G_c value has decreased compared to the HD1CG sample. But the PDI value of these two samples is comparable with the HDPE sample. It is believed that increasing the amount of GNPs increases the possibility of agglomeration, and this leads to antioxidants being trapped between graphene nanosheets during processing. As can be seen in Table 3, HD6SG and HD3SG samples, the amount of G_c has increased more than HDPE sample. Surprisingly, the OIT of these samples (HD3SG and HD6SG) is lower than that of the HDPE neat sample. It is believed that due to SG's high polarity, antioxidants are highly absorbed on graphene surfaces or trapped between agglomerates. This causes the antioxidants to not function properly during processing, and this leads to polymer deterioration and the subsequent increase of the crossover modulus.

Preprint not peer reviewed

This preprint research paper has not been peer reviewed. Electronic copy available at: https://ssrn.com/abstract=4698229

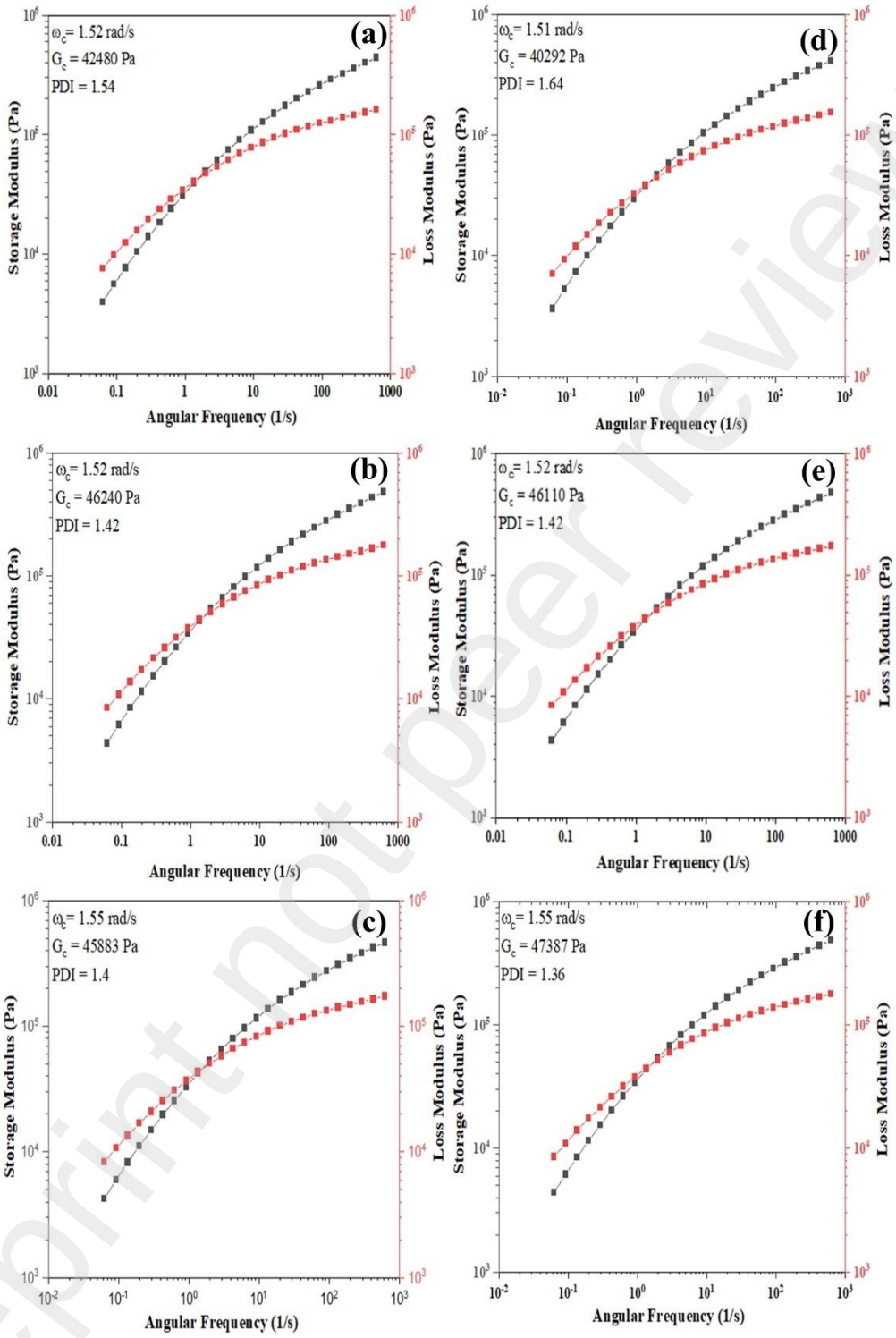

Fig. 7 The melt rheological measurement as function of SG/CG content and frequency: (a) HD1CG, (b) HD3CG, (c) HD6CG, (d) HD1SG, (e) HD3SG, and (f) HD6SG.

Preprint not peer reviewed

This preprint research paper has not been peer reviewed. Electronic copy available at: https://ssrn.com/abstract=4698229

Table 3. The melt rheological results of samples

Samples	Crossing angular frequency point (1/s)	Crossing modulus point (Pa)	Mean relaxation time (s)	PDI
HDPE	1.55	44674	0.65	1.44
HD1SG	1.51	40292	0.66	1.64
HD3SG	1.52	46110	0.66	1.42
HD6SG	1.55	47387	0.65	1.36
HD1CG	1.52	42480	0.66	1.54
HD3CG	1.42	46240	0.7	1.42
HD6CG	1.55	45883	0.65	1.4

2.2.4. Degradation in ClO_2-containing water

Due to the fact that graphene nanoplatelets (CG) are more interfacially adherent to PE100 matrix than SG, PE/CG composites were selected for further investigation of thermo-oxidative stability in chlorinated media. As a means of gaining a deeper understanding into surface processes during aging in ClO_2 solution, FESEM analyses were conducted. Fig. 8 shows the resulting images. As shown in Fig. 8-a, b, c, and d, a higher surface roughness was observed after only three weeks of HDPE exposure, and surface micro cracks appeared. As the ClO* radical could be present in the dilute solution of ClO_2, at the surface of direct contact, this radical could interact indiscriminately with the AO and the chains of the polymer. This could result in advanced highly local material embrittlement [15]. According to Colin et al. [11], It has previously been demonstrated that PE

Preprint not peer reviewed

This preprint research paper has not been peer reviewed. Electronic copy available at: https://ssrn.com/abstract=4698229

will become brittle when its weight average molar mass (M_W) is below a threshold value of 70 $gmol^{-1}$, without regard to its initial morphology. In order to remove hydrogen atoms from the molecules of a polymer, ClO_2 is not sufficiently reactive [12, 17]. In order to resolve this perceived conflict, a conceptual model can be developed based on ClO_2's physical and chemical characteristics. ClO_2 is dissolved in water as a non-dissociated dissolved gas [12, 55, 56]. The radical is also thermodynamically unstable in solution and possesses an electron configuration that allows it to persist over an extended period of time [57]. ClO_2 in water produces almost exclusively ionic compounds. As a result, these ions cannot penetrate the bulk due to their hydrate shells which act as sterical barriers. ClO_2 migration into the polymer appears to be possible. To describe material deterioration in subsurface layers, Yu et al. [9, 58] recommended chlorine monoxide (ClO*) radicals as active radicals that react with the polymer formed by AO and ClO_2. Furthermore, Hassinen and Jacobson [59] suggested that ClO_2 may produce proxy radicals from hydroperoxides, which would shorten the initial occurrence time of radical chain break. According to the above assumption, both scenarios are based on ClO_2 penetration into the polymer matrix. It is possible that the sporadic presence of surface cracks on HDPE is related to regionally inhibited ClO_2 migration.

An oxidative impact of ClO_2 was clearly verified by means of the conventional methods. Tensile tests showed a distinctive embrittlement of the films as a result of physical (reflect in extinction of yield point) and chemical (decrease of strain at failure due to chain scission) material aging, after comparatively short exposure times at elevated exposure temperatures. The greatest reduction of the elongation at failure (ε_b) is observed for the HDPE specimen (Fig. 9-a). HD6CG showed a smaller decrease in the value of (ε_b) in response to exposure to 5 ppm ClO_2 for three weeks than HD3CG, and HD1CG, as shown in Fig 10. taking ε_b = 100% as an ‘‘end life criterion’’ according

Preprint not peer reviewed

This preprint research paper has not been peer reviewed. Electronic copy available at: https://ssrn.com/abstract=4698229

to colin et al. [10], On the basis of Colin's end life criterion, HD6CG is the most stable sample against ClO_2 followed by HD3CG, HD1CG, and HDPE. According to Colin et al. [11], the degradation process in ClO_2-containing water is diffusion controlled. Because GNP block aqueous solution ClO_2 migration. By acting as a physical barrier, they prevent molecules from diffusing through the thin film [60-63]. This can be observed in the mechanical properties of the aged sample presented in Fig. 9. As CG content increases, a more tortuous barriers are made against of ClO_2. In our opinion, this reason can be one of the controlling factors of the ageing process. On the other hand, as reported in DPPH results, scavenging activity improved gradually, as the GNP concentration continuously increased. Increasing CG concentration results in a greater amount of sp^2 structure and the number of continuous sp^2 hybrid domains involved in radical scavenging. This reason can be another factor of the extreme resistance of HD6CG sample against aggressive ClO_2-containing environment. As an explanation of GNP's role in aging process and mechanism of aging in HDPE and HD6CG samples, Fig. 10 illustrates the schematic of the process.

Preprint not peer reviewed

This preprint research paper has not been peer reviewed. Electronic copy available at: https://ssrn.com/abstract=4698229

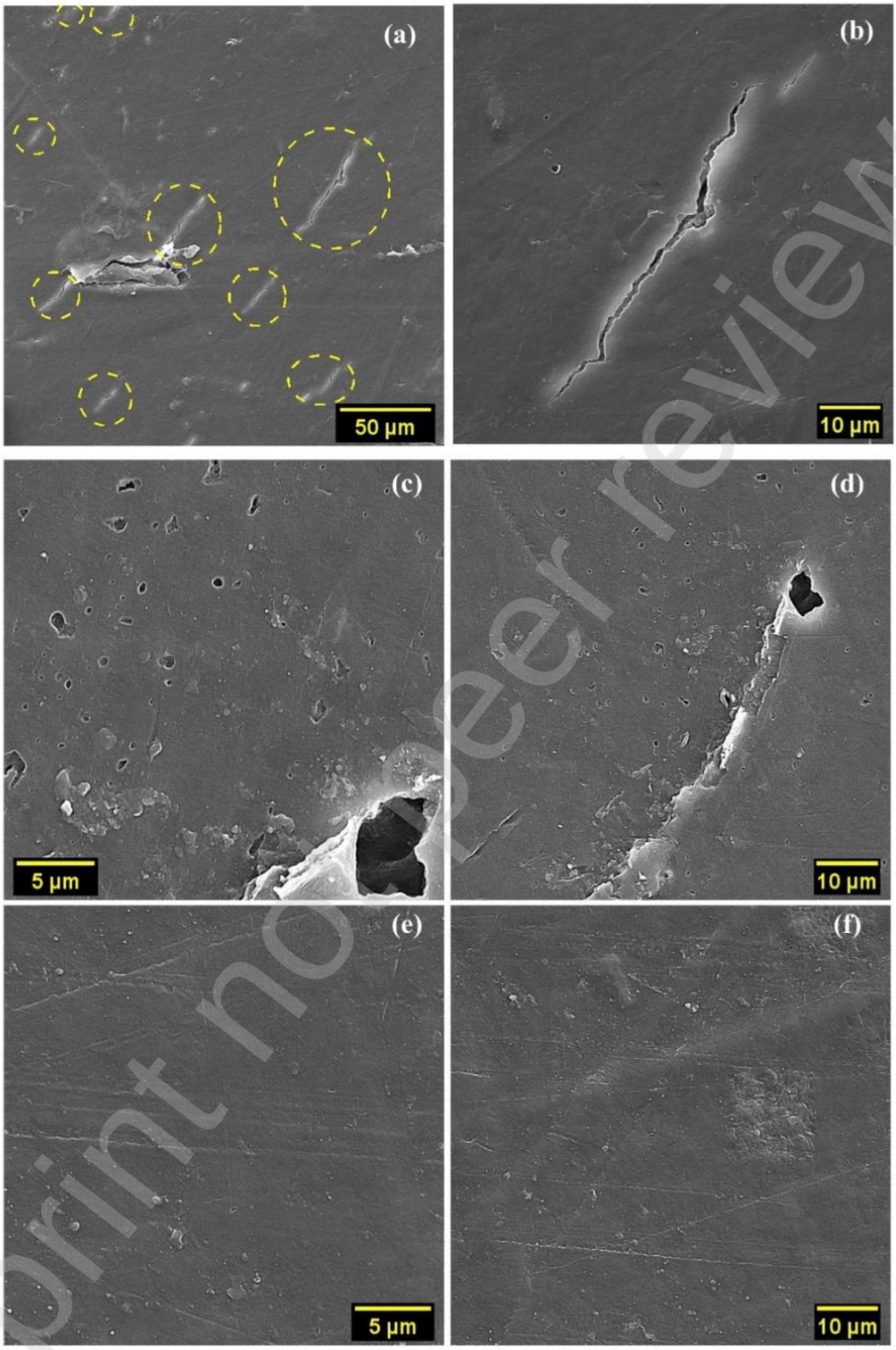

Fig. 8 Surface SEM images of (a), (b), (c), and (d) aged HDPE and (e) and (f) aged HD6CG after exposure to 5 ppm ClO_2 for 3 weeks of ageing at 50 ^{o}C.

Preprint not peer reviewed

This preprint research paper has not been peer reviewed. Electronic copy available at: https://ssrn.com/abstract=4698229

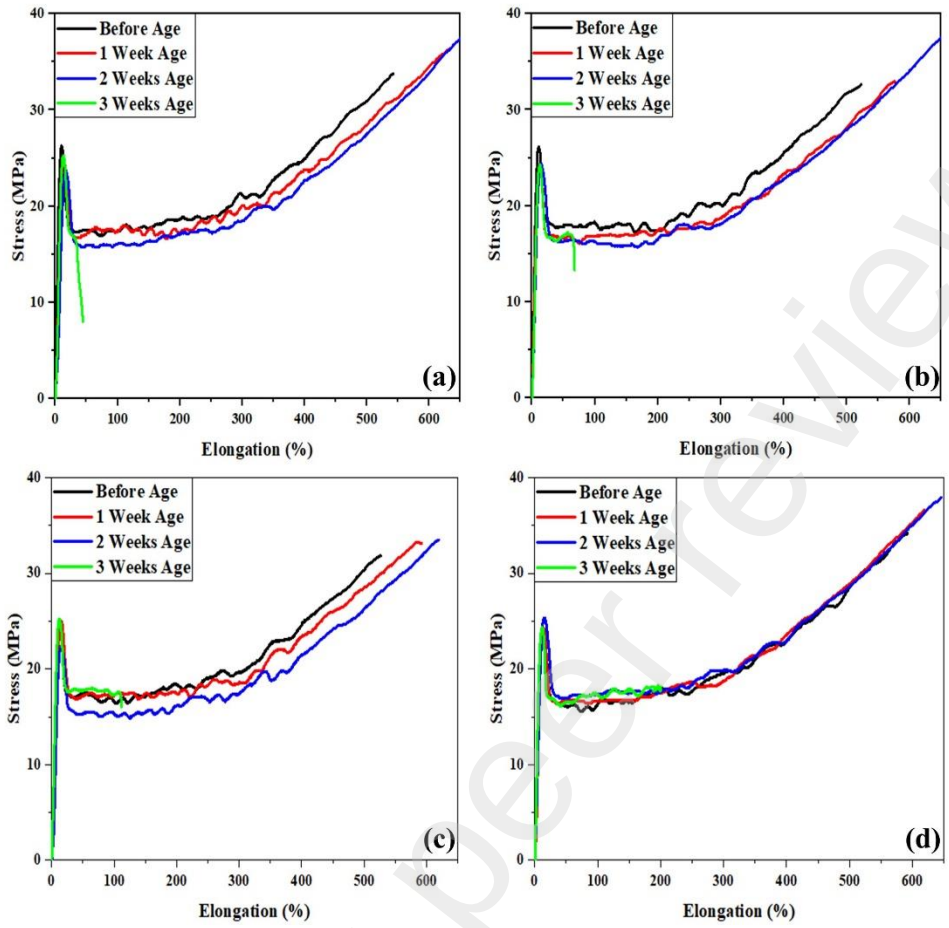

Fig. 9 Tensile curves of (a) aged HDPE films, (b) aged HD1CG, (c) aged HD3CG, and (d) aged HD6CG after exposure to 5 ppm ClO_2 for 3 weeks of ageing at 50 ^oC.

Preprint not peer reviewed

This preprint research paper has not been peer reviewed. Electronic copy available at: https://ssrn.com/abstract=4698229

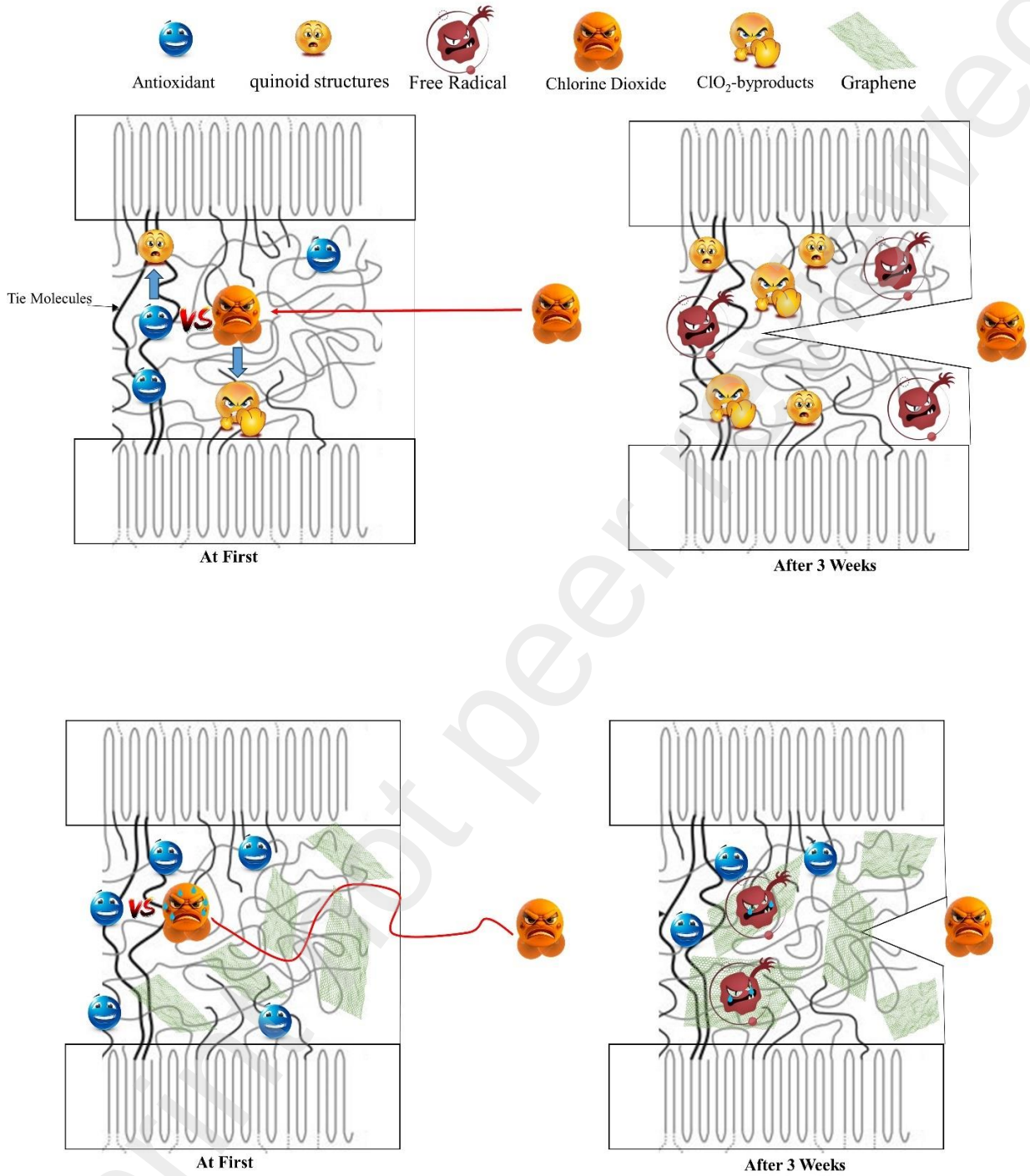

Fig. 10 Schematic of the mechanism for the effect of GNP on aging process and mechanism of aging in HDPE and HD6CG.

Preprint not peer reviewed

This preprint research paper has not been peer reviewed. Electronic copy available at: https://ssrn.com/abstract=4698229

3. Conclusion

Two kinds of graphene nanoplatelets, SG: high polarity and CG: low polarity were added to bimodal high density polyethylene (PE100), in order to improve its resistance against polymer degradation in ClO_2-containing water. Based on OIT measurements, it was evident that PE100 thermo-oxidative stability was significantly enhanced by simultaneously incorporating traditional primary and secondary antioxidants and 0.1 wt.% of CG.

This synergistic thermal stabilization effect of CG is due to its tortuous path effect, free radical scavenging ability, physical barrier effect on degradation product emmission, and thermal conductivity improvements. Consequently, the proper nanofiller and antioxidant probably produced antioxidant synergy, preventing polymer thermo-oxidation degradation during melt proccessing, which is also confirmed with rheological measurements.

As a result of ageing for three weeks in chlorine dioxide containing water, sample having 0.6 wt.% of CG showed a 200 percent elongation at break after 3 weeks of ageing in hot chlorine dioxide containing water, while the neat sample shows only 50% under the same condition. This result confirm the role of low polar GNP on stabilization of polyethylene against chemical degradation of chlorine dioxide. Tortuous barriers are formed against ClO_2 and radical scavenging of sp^2 structure of CG is the reason of the extreme resistance of HD6CG sample against aggressive ClO_2-containing environment. Comparing the results of 0.1 wt.% and 0.6wt.% containing CG samples, it can be concluded that for chemical degradation protection a certain amount of nanofiller with good dispersion is required. Based on the presented results, low polar GNP is a powerful material that can play a multifunctional role in regulating the structure-property relationship of advaced

Preprint not peer reviewed

This preprint research paper has not been peer reviewed. Electronic copy available at: https://ssrn.com/abstract=4698229

polymer/GNP nanocomposites. It has the potential to be an economical metod to extend PE100 pipes' life.

Preprint not peer reviewed

This preprint research paper has not been peer reviewed. Electronic copy available at: https://ssrn.com/abstract=4698229

Refrences

[1] G. Pircheraghi, A. Sarafpour, R. Rashedi, K. Afzali, M. Adibfar, Correlation between rheological and mechanical properties of black PE100 compounds-Effect of carbon black masterbatch, eXPRESS Polymer Letters 11(8) (2017).
[2] A. Sarafpour, G. Pircheraghi, R. Rashedi, K. Afzali, Correlation between isothermal crystallization and morphological/rheological properties of bimodal polyethylene/carbon black systems, Polymer Crystallization 1(3) (2018) e10014.
[3] M. Bredács, A. Redhead, A. Frank, A. Bastero, G. Pinter, Development and implementation of an accelerated method for chlorine dioxide exposure, AIP Conference Proceedings, AIP Publishing LLC, 2016, p. 070009.
[4] M. Bredacs, Aging Mechanism and Material Ranking of PE Pipe Grades in Aqueous Chlorine Dioxide and Hypochlorite Solutions, University of Leoben, 2020.
[5] A. Vertova, A. Miani, G. Lesma, S. Rondinini, A. Minguzzi, L. Falciola, M.A. Ortenzi, Chlorine dioxide degradation issues on metal and plastic water pipes tested in parallel in a semi-closed system, International Journal of Environmental Research and Public Health 16(22) (2019) 4582.
[6] A. Redhead, A. Frank, G. Pinter, Accelerated investigation of the effect of chlorine dioxide on the long-term failure behavior and the material aging of polyethylene for raised temperature resistance, Proceedings of Plastic Pipes XVI Conference 2012, 2012, pp. 1-10.
[7] W. Yu, T. Reitberger, T. Hjertberg, J. Oderkerk, F. Costa, U.W. Gedde, Antioxidant consumption in squalane and polyethylene exposed to chlorinated aqueous media, Polymer degradation and stability 97(11) (2012) 2370-2377.
[8] P. Wardman, Reduction potentials of one-electron couples involving free radicals in aqueous solution, Journal of Physical and Chemical Reference Data 18(4) (1989) 1637-1755.
[9] W. Yu, T. Reitberger, T. Hjertberg, J. Oderkerk, F. Costa, V. Englund, U.W. Gedde, Chlorine dioxide resistance of different phenolic antioxidants in polyethylene, Polymer degradation and stability 111 (2015) 1-6.
[10] X. Colin, L. Audouin, J. Verdu, M. Rozental-Evesque, B. Rabaud, F. Martin, F. Bourgine, Aging of polyethylene pipes transporting drinking water disinfected by chlorine dioxide. I. Chemical aspects, Polymer Engineering & Science 49(7) (2009) 1429-1437.
[11] X. Colin, L. Audouin, J. Verdu, M. Rozental-Evesque, B. Rabaud, F. Martin, F. Bourgine, Aging of polyethylene pipes transporting drinking water disinfected by chlorine dioxide. Part II—Lifetime prediction, Polymer Engineering & Science 49(8) (2009) 1642-1652.
[12] J. Hoigne, H. Bader, Kinetics of reactions of chlorine dioxide with representative micropollutants in water, Vom Wasser 59 (1982) 253-267.
[13] R.G. Rice, J.A. Cotruvo, Ozone/chlorine dioxide oxidation products of organic materials. Proceedings of a conference held in Cincinnati, Ohio, November 17-19, 1976, (1978).
[14] J. Atkinson, Chemical oxidation in water treatment, NINTH CONGRESS 11-14 September, 1972, p. 1.
[15] M. Bredács, A. Frank, A. Bastero, A. Stolarz, G. Pinter, Aging Mechanism of Polyethylene Pipe Material in Chlorine Dioxide and Hypochlorite Solution, Proceedings Plastics Pipes XIX2018.
[16] N. Lancioni, M. Parlapiano, M. Sgroi, L. Giorgi, V. Fusi, G. Darvini, L. Soldini, B. Szeląg, A.L. Eusebi, F. Fatone, Polyethylene pipes exposed to chlorine dioxide in drinking water supply system: A critical review of degradation mechanisms and accelerated aging methods, Water Research (2023) 120030.
[17] A.A. Stevens, Reaction products of chlorine dioxide, Environmental Health Perspectives 46 (1982) 101-110.

Preprint not peer reviewed

This preprint research paper has not been peer reviewed. Electronic copy available at: https://ssrn.com/abstract=4698229

[18] B.O. Lindgren, C.M. Svahn, G. Widmark, Chlorine dioxide oxidation of cyclohexene, Acta Chem. Scand 19(1) (1965) 7.
[19] B.O. Lindgren, C.M. Svahn, Reactions of chlorine dioxide with unsaturated compounds. II. Methyl oleate, Acta Chem. Scand 20(1) (1966).
[20] W. Yu, B. Azhdar, D. Andersson, T. Reitberger, J. Hassinen, T. Hjertberg, U. Gedde, Deterioration of polyethylene pipes exposed to water containing chlorine dioxide, Polymer degradation and stability 96(5) (2011) 790-797.
[21] J. Bolland, G. Gee, Kinetic studies in the chemistry of rubber and related materials. II. The kinetics of oxidation of unconjugated olefins, Transactions of the Faraday Society 42 (1946) 236-243.
[22] J. Bolland, G. Gee, Kinetic studies in the chemistry of rubber and related materials. III. Thermochemistry and mechanisms of olefin oxidation, Transactions of the Faraday Society 42 (1946) 244-252.
[23] B. Yuan, C. Bao, L. Song, N. Hong, K.M. Liew, Y. Hu, Preparation of functionalized graphene oxide/polypropylene nanocomposite with significantly improved thermal stability and studies on the crystallization behavior and mechanical properties, Chemical Engineering Journal 237 (2014) 411-420.
[24] B. Yuan, Y. Zhan, S. Sheng, P. Li, H. Zhao, Y. He, Exploration on the influence mechanism of heteroatom doped graphene on thermal oxidative stability and decomposition of polypropylene, Materials Today Communications 25 (2020) 101446.
[25] J. Bu, X. Huang, S. Li, P. Jiang, Significantly enhancing the thermal oxidative stability while remaining the excellent electrical insulating property of low density polyethylene by addition of antioxidant functionalized graphene oxide, Carbon 106 (2016) 218-227.
[26] S. Liu, J. Yao, Q. Liu, Y. Huang, M. Kong, Q. Yang, G. Li, Tuning the physicochemical structure of graphene oxide by thermal reduction temperature for improved stabilization ability toward polymer degradation, The Journal of Physical Chemistry C 124(16) (2020) 8999-9008.
[27] J. Yang, Y. Huang, Y. Lv, S. Li, Q. Yang, G. Li, The synergistic mechanism of thermally reduced graphene oxide and antioxidant in improving the thermo-oxidative stability of polypropylene, Carbon 89 (2015) 340-349.
[28] R. Li, K. Shi, L. Ye, G. Li, Polyamide 6/graphene oxide-g-hindered phenol antioxidant nano-composites: Intercalation structure and synergistic thermal oxidative stabilization effect, Composites Part B: Engineering 162 (2019) 11-20.
[29] M. Li, Y.G. Jeong, Poly (ethylene terephthalate)/exfoliated graphite nanocomposites with improved thermal stability, mechanical and electrical properties, Composites Part A: Applied Science and Manufacturing 42(5) (2011) 560-566.
[30] Y. Lin, Y. Liu, D. Zhang, C. Chen, G. Wu, Radiation resistance of poly (methyl methacrylate)/reduced graphene oxide nanocomposites fabricated through latex mixing and in situ reduction, Chemical Engineering Journal 315 (2017) 516-526.
[31] K. Parvez, Z.-S. Wu, R. Li, X. Liu, R. Graf, X. Feng, K. Müllen, Exfoliation of graphite into graphene in aqueous solutions of inorganic salts, Journal of the American Chemical Society 136(16) (2014) 6083-6091.
[32] M. Goodarzi, G. Pircheraghi, H.A. Khonakdar, Tailoring the graphene polarity through the facile and one-step electrochemical exfoliation in low concentration of exfoliation agents, FlatChem 22 (2020) 100181.
[33] A. Dordinejad, F. Sharif, M. Ebrahimi, R. Rashedi, Time-sweep rheometry for evaluating polyethylene degradation behavior: Effect of formulation and process conditions, Polymer Testing 70 (2018) 39-46.
[34] N. Baali, A. Khecha, A. Bensouici, G. Speranza, N. Hamdouni, Assessment of antioxidant activity of pure graphene oxide (GO) and ZnO-decorated reduced graphene oxide (rGO) using DPPH radical and H2O2 scavenging assays, C 5(4) (2019) 75.

Preprint not peer reviewed

This preprint research paper has not been peer reviewed. Electronic copy available at: https://ssrn.com/abstract=4698229

[35] I.A. Ahmad, K.K. Koziol, S. Deveci, H.-K. Kim, R.V. Kumar, Advancing the use of high-performance graphene-based multimodal polymer nanocomposite at scale, Nanomaterials 8(11) (2018) 947.
[36] I.A. Ahmad, H.-K. Kim, S. Deveci, R.V. Kumar, Non-isothermal crystallisation kinetics of carbon black-graphene-based multimodal-polyethylene nanocomposites, Nanomaterials 9(1) (2019) 110.
[37] I.A.I.A. Ahmad, Multimodal Polyethylene-Graphene Nanocomposite via Melt Extrusion, University of Cambridge, 2019.
[38] Z. Hu, Y. Chen, Q. Hou, R. Yin, F. Liu, H. Chen, Characterization of graphite oxide after heat treatment, New Journal of Chemistry 36(6) (2012) 1373-1377.
[39] N. Gharbi, M. Pressac, M. Hadchouel, H. Szwarc, S.R. Wilson, F. Moussa, [60] Fullerene is a powerful antioxidant in vivo with no acute or subacute toxicity, Nano Letters 5(12) (2005) 2578-2585.
[40] P. Watts, P. Fearon, W. Hsu, N. Billingham, H. Kroto, D. Walton, Carbon nanotubes as polymer antioxidants, Journal of Materials Chemistry 13(3) (2003) 491-495.
[41] Y. Qiu, Z. Wang, A.C. Owens, I. Kulaots, Y. Chen, A.B. Kane, R.H. Hurt, Antioxidant chemistry of graphene-based materials and its role in oxidation protection technology, Nanoscale 6(20) (2014) 11744-11755.
[42] S.H. Lee, E. Cho, S.H. Jeon, J.R. Youn, Rheological and electrical properties of polypropylene composites containing functionalized multi-walled carbon nanotubes and compatibilizers, Carbon 45(14) (2007) 2810-2822.
[43] S. Park, S. He, J. Wang, A. Stein, C.W. Macosko, Graphene-polyethylene nanocomposites: Effect of graphene functionalization, Polymer 104 (2016) 1-9.
[44] J. Yang, Y. Huang, Y. Lv, P. Zhao, Q. Yang, G. Li, The intrinsic thermal-oxidative stabilization effect of chemically reduced graphene oxide on polypropylene, Journal of Materials Chemistry A 1(37) (2013) 11184-11191.
[45] S. Nawaz, P. Nordell, H. Hillborg, U.W. Gedde, Antioxidant activity in aluminium oxide–poly (ethylene-co-butyl acrylate) nanocomposites, Polymer degradation and stability 97(6) (2012) 1017-1025.
[46] N. Allen, M. Edge, T. Corrales, A. Childs, C. Liauw, F. Catalina, C. Peinado, A. Minihan, Entrapment of stabilisers in silica: I. Controlled release of additives during polypropylene degradation, Polymer degradation and stability 56(2) (1997) 125-139.
[47] S. Morlat-Therias, B. Mailhot, D. Gonzalez, J.-L. Gardette, Photooxidation of polypropylene/montmorillonite nanocomposites. 2. Interactions with antioxidants, Chemistry of Materials 17(5) (2005) 1072-1078.
[48] A. D'silva, Adsorption of antioxidants by carbon blacks, Carbon 36(9) (1998) 1317-1325.
[49] N.L. Batista, E. Helal, R.S. Kurusu, N. Moghimian, E. David, N.R. Demarquette, P. Hubert, Mass-produced graphene—HDPE nanocomposites: thermal, rheological, electrical, and mechanical properties, Polymer Engineering & Science 59(4) (2019) 675-682.
[50] Y. Lan, H. Liu, X. Cao, S. Zhao, K. Dai, X. Yan, G. Zheng, C. Liu, C. Shen, Z. Guo, Electrically conductive thermoplastic polyurethane/polypropylene nanocomposites with selectively distributed graphene, Polymer 97 (2016) 11-19.
[51] H. Shin, M.-Y. Lim, S. Kong, S. Kim, S.W. Lee, Y. Lee, J.-C. Lee, Improving Physical Properties of Polypropylene Nanocomposites by a Natural Resource-Based Bottom-up Graphene Oxide Filler, Macromolecular Research 29 (2021) 487-493.
[52] F.R. Costa, U. Wagenknecht, D. Jehnichen, M.A. Goad, G. Heinrich, Nanocomposites based on polyethylene and Mg–Al layered double hydroxide. Part II. Rheological characterization, Polymer 47(5) (2006) 1649-1660.
[53] E. Miller, J.P. Rothstein, Control of the sharkskin instability in the extrusion of polymer melts using induced temperature gradients, Rheologica acta 44 (2004) 160-173.

Preprint not peer reviewed

This preprint research paper has not been peer reviewed. Electronic copy available at: https://ssrn.com/abstract=4698229

[54] T. Mezger, The rheology handbook: for users of rotational and oscillatory rheometers, European Coatings2020.
[55] G. Gordon, R.G. Kieffer, D.H. Rosenblatt, The chemistry of chlorine dioxide, Progress in inorganic chemistry 15 (1972) 201-286.
[56] J. Myhrstad, J. Samdal, Behavior and determination of chlorine dioxide, Journal-American Water Works Association 61(4) (1969) 205-208.
[57] M. Bredács, A. Frank, A. Bastero, A. Stolarz, G. Pinter, Accelerated aging of polyethylene pipe grades in aqueous chlorine dioxide at constant concentration, Polymer Degradation and Stability 157 (2018) 80-89.
[58] W. Yu, E. Sedghi, S. Nawaz, T. Hjertberg, J. Oderkerk, F. Costa, U. Gedde, Assessing the long-term performance of polyethylene stabilised with phenolic antioxidants exposed to water containing chlorine dioxide, Polymer testing 32(2) (2013) 359-365.
[59] J. Hassinen, K. Jacobson, Investigation and Comparison of Accelerated Pipe Testing Data with True Pipe Installations in Contact with Chlorine Dioxide as Disinfectant, Conference proceedings Plastic Pipes Conference XVI, 2012.
[60] S. Bellucci, Study of Graphene Epoxy/Nanoplatelets Thin Films Subjected to Aging in Corrosive Environments, Journal of Composites Science 6(2) (2022) 39.
[61] W. Sun, Y. Yang, Z. Yang, L. Wang, J. Wang, D. Xu, G. Liu, Review on the corrosion-promotion activity of graphene and its inhibition, Journal of Materials Science & Technology 91 (2021) 278-306.
[62] Y. Zhang, J. Sun, X. Xiao, N. Wang, G. Meng, L. Gu, Graphene-like two-dimensional nanosheets-based anticorrosive coatings: A review, Journal of Materials Science & Technology 129 (2022) 139-162.
[63] X. Hu, Y. Zhang, C. Liu, H. Cui, Polydopamine wrapped polyaniline nanosheets: synthesis and anticorrosion application for waterborne epoxy coatings, Journal of Materials Science & Technology (2023).

Preprint not peer reviewed

This preprint research paper has not been peer reviewed. Electronic copy available at: https://ssrn.com/abstract=4698229